Magnetic properties of pure and diamagnetically doped jarosites: Model *kagomé* antiferromagnets with variable coverage of the magnetic lattice

A. S. Wills* and A. Harrison†
Department of Chemistry, The University of Edinburgh, The King's Buildings, West Mains Road, Edinburgh EH9 3JJ, United Kingdom

C. Ritter
Institut Laue-Langevin, Avenue des Martyrs, Boîte Postale 156, 38042 Grenoble Cedex 9, France

R. I. Smith
ISIS Facility, Rutherford Appleton Laboratory, Chilton, Didcot, Oxon OX11 0QX, United Kingdom
(Received 17 August 1999)

Jarosites are a family of minerals of general formula $AFe_3(OH)_6(SO_4)_2$ (where A^+ is typically a univalent cation such as Na^+, K^+, Rb^+, ND_4^+, Ag^+, Tl^+, or D_3O^+). They provide good model Heisenberg *kagomé* antiferromagnets with which to test suggestions that highly frustrated antiferromagnets have unconventional magnetic ground states and excitations. In all cases Fe^{3+} ions provide $S=\frac{5}{2}$ moments, arranged on the vertices of well-separated *kagomé* layers, and are coupled through strong antiferromagnetic exchange with values of the Weiss constants θ of the order of -700 K. We report dc magnetic susceptibility (χ_{dc}) and powder neutron diffraction studies of materials in which $A^+=Na^+$, Rb^+, ND_4^+, Ag^+, or D_3O^+ and show that for all materials except the deuteronium ($A^+=D_3O^+$) salt, long-range magnetic order with the in-plane $q=0$ spin structure sets in below a temperature T_f of the order of 50 K. $(D_3O)Fe_3(SO_4)_2(OD)_6$ shows only a spin-glass-like transition at $T_f \cong 15$ K. There is no obvious difference in the structures of the salts that show magnetic long-range order, and the deuteronium salt except for the coverage of the magnetic lattice, which is higher ($97\pm3\%$) in the latter than that of the rest of the family ($\leqslant 95\%$, and most typically $\cong 90\%$). It is proposed that reduction of the coverage of the magnetic lattice induces long-range order in the jarosites, and the material $(D_3O)Fe_{3-x}Al_y(OD)_6(SO_4)_2$, in which the coverage of the magnetic lattice is $89\pm3\%$ has been prepared and characterized to test this hypothesis. χ_{dc} for this material has a cusp at 25.5 K, and powder neutron diffraction reveals long-range magnetic order at 1.4 K with the same ordering vector as that seen in the other materials.

I. INTRODUCTION

Frustration confers unusual cooperative properties on a lattice of exchange-coupled moments.[1–4] In the simple case of a triangular lattice of Heisenberg spins with antiferromagnetic nearest-neighbor exchange, frustration leads to a 120° array [Fig. 1(a)] which possesses a double degeneracy associated with the handedness, or *chirality* of the vector array in addition to the trivial degeneracy associated with the global rotation of spins; the second, degenerate form is shown in Fig. 1(b). While this extra degree of freedom, which behaves as an Ising variable, bestows new critical properties on the spin lattice,[5–7] the ground state and excitations are believed to be conventional. The spin configuration depicted in Figs. 1(a) or 1(b) may be extended infinitely in the plane of the paper in a unique fashion to produce a long-range ordered array [Fig. 2(a)], and this is believed to be the ground state of this form of antiferromagnet for $S>\frac{1}{2}$ (for $S=\frac{1}{2}$ there is still some debate about whether this Néel state is the true ground state, or whether a resonating valence bond or spin fluid ground state is preferred instead[8–10]). However, when the triangular plaquettes are connected through shared vertices to form the *kagomé* lattice, shown in Fig. 2(b), the order within an isolated plaquette cannot be propagated in an unambiguous fashion. This figure also displays one of the manifold of possible spin states which satisfies the requirement that all spins are at 120° to each other, the so-called $q=0$ state;[10–12] another highly symmetric array whose energy is the same to first order is shown in Fig. 2(c) and is called the $\sqrt{3}\times\sqrt{3}$ state on account of the relative size of the magnetic and nuclear cells. It is only when further-neighbor exchange interactions are introduced,[12] or thermal[13,14] or quantum[15–17] fluctuations incorporated in the model that a subset of the manifold of ground states is selected. For classical (large) spins, small quantum or thermal fluctuations appear to select configurations in which all spins are coplanar, and within this subset of configurations, $\sqrt{3}\times\sqrt{3}$ order is probably selected as $T\rightarrow 0$.[12–14,18]

Despite the fascination this lattice holds, there are remarkably few experimental systems with which to study its properties and test theory. The majority of experimental work has been on the magnetoplumbite isomorph $SrCr_xGa_{12-x}O_{19}$ [SCGO(x)][19–29] which contains a *kagomé* lattice of Cr^{3+} ions which behave as strongly antiferromagnetically coupled Heisenberg spins $\frac{3}{2}$ (the Weiss constant $\theta \approx -500$ K). A spin-glass-like transition is observed in both the dc and ac magnetic susceptibility (χ_{dc} and χ_{ac}, respectively) on cooling, where the freezing temperature depends on the coverage of the magnetic lattice; for a sample with 89% coverage of the *kagomé* lattice, $T_f=3.5$ K. Extrapolation of T_f with coverage gives a value of $T_f=4.15$ K for the pure lattice.[20,23,24] However, the nature of this frozen phase is unconventional: the heat capacity evolves with temperature

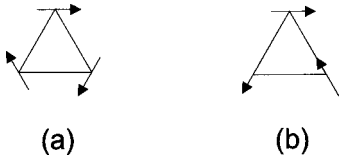

FIG. 1. Triangular plaquatte of antiferromagnetically coupled moments free to rotate in the plane of the paper (a) and (b) show degenerate spin configurations of minimum energy and opposite chirality.

as T^2 rather than the approximately linear dependence associated with conventional spin glasses; neutron scattering data for samples with 79 and 92% coverage of the *kagomé* lattices suggest that at least 50% of the moments continue to fluctuate strongly well below T_f.[21,27] This observation is further supported by muon spin relaxation (μSR) measurements.[30] However, these data also highlight one of the problems encountered when working with SCGO(x)—the coverage of the *kagomé* lattice with magnetic atoms depends on the preparative conditions and is typically $\leqslant 89\%$.[23,24] The magnetic lattice is also somewhat more complex than the simple model studied by theorists; a pair of kagome layers forms a sandwich with an additional triangular layer in the middle so that the magnetic system is best described as a disordered pyrochlore slab.[26] Thus, although SCGO(x) is a fascinating example of a highly frustrated antiferromagnet, and can now be synthesised with essentially complete coverage of the magnetic lattice[24] it is not a close replica of the model system studied by theorists.

There are a number of other systems that have been put forward as model *kagomé* antiferromagnets. The collection of nuclear spin-$\frac{1}{2}$ moments provided by ^{3}He absorbed at certain densities on graphite[31,32] is one such case. However, recent theoretical work[33] suggests that this system is more complex than previously thought, and multiple spin exchange effects appear to play an important role in the collective magnetic properties such that it can no longer be regarded as a simple *kagomé* antiferromagnet. The $S=1$ organic antiferromagnet m-MPYNN$\cdot BF_4$ (where m-MPYNN is m-N-methylpyridium α-nitronyl nitroxide)[34,35] has also been put forward as a model material, and holds much promise, though the low spin density and high degree of hydrogenation create experimental difficulties in neutron scattering experiments. Possibly the most promising, and certainly the largest class of compounds that might serve as model *kagomé* antiferromagnets is the Jarosite family of minerals $AFe_3(OH)_6(SO_4)_2$ (where A^+ is a univalent cation such as Na^+, K^+, Rb^+, NH_4^+, Ag^+, Tl^+, or H_3O^+, or stoichiometric quantities of the divalent cations $\frac{1}{2}Pb^{2+}$ or $\frac{1}{2}Hg^{2+}$), and the isomorphic families in which Fe^{3+} is exchanged for other trivalent ions such as Cr^{3+} or V^{3+} or the sulfate group is exchanged for SeO_4^{2-} or CrO_4^{2-}.[36,37]

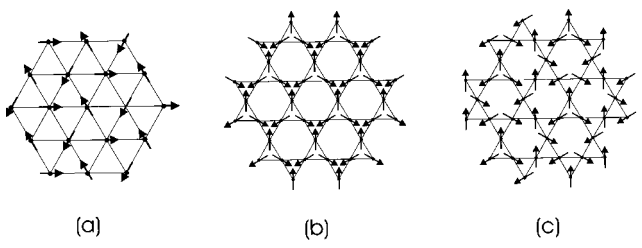

FIG. 2. (a) Triangular lattice with Néel array of spins and *kagomé* lattices with (b) $q=0$ and (c) $\sqrt{3}\times\sqrt{3}$ spin arrays.

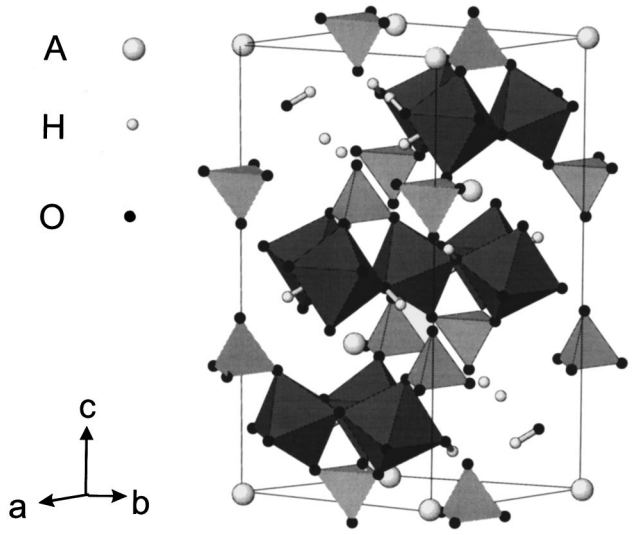

FIG. 3. Crystal structure of sodium jarosite, depicting the disposition of FeO_6 octahedra and sulfate tetrahedra, and marking the boundaries of the nuclear unit cell. Some atoms outside the unit cell are also included to complete all coordination polyhedra.

Jarosites have been studied by mineralogists as important sulfur-bearing minerals, and there is extensive documentation of their structure, stoichiometry and syntheses;[38–40] they are also of industrial importance as a means of precipitating iron from solutions bearing a mixture of metal ions,[36] and the silver salt is a significant ore of that element.[41] The unit cell of hydronium jarosite is shown in Fig. 3 which depicts layers of vertex-sharing Fe-O octahedra stacked along the c axis and well separated by sulfate and hydronium ions. A clearer illustration of the *kagomé* lattice of Fe^{3+} ions is given in Fig. 4 which shows the Fe-O octahedra for one layer viewed

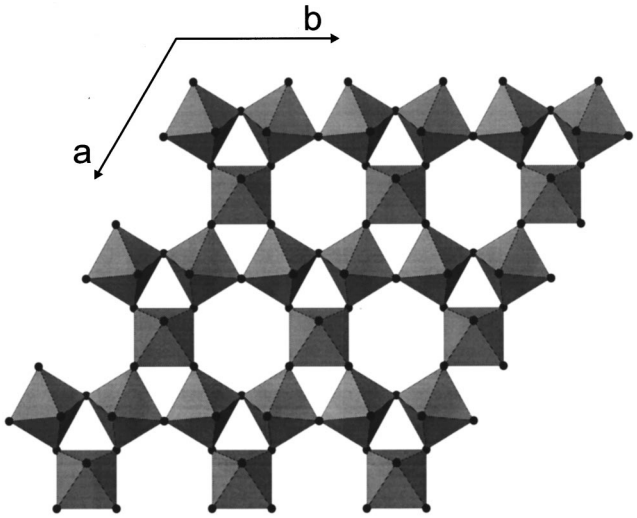

FIG. 4. Single layer of Fe-O coordination octahedra viewed along the c axis of a jarosite with the iron atom at the center of each octahedron.

along the crystal *c* axis. However, it is only relatively recently that there has been much interest in the *magnetic* behavior of Jarosites.[37,42–55] It was rapidly established that Fe^{3+} ions have a $^6A_{1g}$ ground term and approximate well to strongly coupled Heisenberg $S=\frac{5}{2}$ spins,[42–44] with Weiss constants of the order of -700 K.[43,44] The structure of these materials gives rise to exchange pathways that are much shorter between vertex-sharing FeO_6 units compared with any other route so it is expected that these materials are good models for the simple Hamiltonian

$$H=J\sum_{i,j}\overline{S_i}\cdot\overline{S_j}, \tag{1}$$

where the exchange constant J is limited to nearest-neighbor spins S_i and S_j within the *kagomé* layers. However, the cooperative magnetic properties of these materials fall into two categories. The majority of the compounds studied to date ($A^+=Na^+$, K^+, NH_4^+, $\frac{1}{2}Pb^{2+}$) show a transition to long-range magnetic order at a temperature of the order of 50 K,[43–45,48] and where it has been studied, the spin array below this temperature has been shown to adopt the $q=0$ configuration within the *kagomé* layers, and these in turn are arranged antiferromagnetically along the *c* axis.[37] In contrast, the hydronium salt ($A^+=H_3O^+$) and its deuterated analog ($A^+=D_3O^+$) show no long-range magnetic order down to 0.4 K.[49–51] Instead, measurements of χ_{dc} indicate a spin glasslike transition at a temperature T_f of the order of 15 K, with a divergence between field-cooled and zero-field-cooled susceptibility (the precise value of T_f depends on whether the material is deuterated and on the preparative conditions[53] and we discuss this point in Sec. IV). Below T_f neutron scattering data indicate that the moments only possess short-range correlations,[50,54] and freeze progressively as the sample is cooled further so that they appear static on a time scale of 10 ps at 1.5 K.[55] It is not clear why this difference between different types of jarosites arises. All the materials are isostructural and there are no obvious correlations between different forms of magnetic behavior and either the cell parameters or exchange geometry between Fe^{3+} ions. The only clear structural or compositional distinction between the hydronium or deuteronium salt and the other members of the family is the degree of coverage of the Fe^{3+} sublattice. The jarosites have a tendency to lose Fe^{3+} ions from the structure as they are precipitated, accompanied by protonation of OH^- groups to form H_2O and thus maintain charge balance. However, the degree of loss of magnetic atoms is much lower for the hydronium and deuteronium salts, being as small as 3%, while the other members of the Jarosite family show losses of typically 7–17%. We discuss this further, together with recent studies of the effect of diamagnetic dilution of hydronium jarosite,[53] in Sec. IV.

In this paper we present magnetic susceptibility and neutron powder diffraction data for jarosites in which the *A* cation is Na^+, ND_4^+, Ag^+, and Rb^+ in order to study the manner in which the cooperative properties depend on the nature of this ion. The coverage of the magnetic lattice of these particular materials ranges from 87 to 95% and in all cases magnetic long-range order with the $q=0$ in-plane structure is observed below a temperature of the order of 50 K. In addition to the magnetic Bragg peaks, diffuse scattering is observed above and below the Néel temperature and this is attributed to short-range correlations in the kagome layers. The location and width of this feature resembles that seen in the high coverage hydronium salt,[50] indicating that the propagation vector and magnetic correlation lengths are similar. We also test the hypothesis that a reduction in coverage of the magnetic lattice may induce long-range order in these compounds by preparing the diamagnetically dilute deuteronium jarosite $(D_3O)Fe_{3-x}Al_y(OD)_6(SO_4)_2$. A sample for which the occupation of the magnetic lattice is $89\pm3\%$, shows a cusp in χ_{dc} at 25.5 K, and powder neutron diffraction data taken at 1.4 K indicate that there is magnetic long-range order when compared with a pattern taken at 30 K.

II. EXPERIMENTAL

A. Chemical synthesis

The magnetic behavior of jarosites is very sensitive to their precise composition,[53] which in turn depends on the preparative conditions, so it is important to be explicit about the details of the synthesis if the work is to be reproduced. We give an outline of the method here, and further details in the Appendix.

Jarosite precipitates are formed by the hydrolysis of strongly acidic solutions (pH 0.5–2) (Refs. 56,57) of Fe^{3+} ions, sulfate ions and the relevant *A* cation. If the pH is too high, the reaction produces amorphous iron hydroxysulfates such as $Fe_4(OH)_{10}SO_4$ (Refs. 58,59) and low pH is found to retard the precipitation reaction. In the preparation of all the pure jarosites, the source of iron was the hydrated iron sulfate $Fe_2(SO_4)_2\,nH_2O$ (where $n\approx5$), while the *A* cation was introduced as the anhydrous sulfate. Both these salts were dissolved in D_2O and then heated in PTFE-lined stainless-steel bombs in a precision furnace (Perkin Elmer) with a temperature stability of ±0.5 °C. The result was a partly deuterated material suitable for powder neutron diffraction measurements. The reaction is found to be subject to the kinetic isotope effect and the amount of deuterated precipitate is severely reduced with respect to the protonated product.

The resulting jarosite phases were washed with D_2O and dried at 120 °C for 3–4 h. Powder x-ray diffraction analysis showed all of the materials synthesised to have the $R\bar{3}m$ alunite structure and there was no evidence of any crystalline impurity phases or unreacted starting materials. There was also no evidence for red amorphous iron hydroxy sulfate contaminant and the precipitates all had the characteristic rapid settling time of the jarosites.[36]

The S and D (or H) contents were determined by elemental combustion analysis (Perkin Elmer 240C), while the metal content was determined with an atomic absorption spectrometer (Atomscan, Thermoelectron) equipped with an argon plasma torch. Solutions were prepared by boiling the sample in concentrated HCl to which a small amount of concentrated HNO_3 had been added. The O content was then deduced by subtraction, and the overall stoichiometry determined with the assumption that the S content is stoichiometric.[60] The principal error arises from the metal analysis (±1.0 wt. %) and these are worked through to give the error in the coverage of the Fe sites. The elemental compositions and stoichiometries of the jarosites used in these

TABLE I. Elemental compositions of samples studied in this work; values marked with an asterisk were determined by neutron diffraction (Refs. 49–51) and estimated standard deviations are shown in brackets.

Idealized formula	Elemental composition/wt. %	Stoichiometric formula	Occupation of *kagomé* lattice by magnetic ions
$(H_3O)Fe_3(SO_4)_2(OH)_6$	2.1 H, 34.2 Fe, 13.7 S, 50.0 O	$Fe_{2.84}H_{9.77}S_{2.00}O_{14.56}$	95±4%, 97.3(6)%*
$(D_3O)Fe_3(SO_4)_2(OD)_6$	1.7 D, 36.5 Fe, 13.8 S, 48.0 O	$Fe_{3.03}D_{3.87}S_{2.00}O_{13.92}$	101±4%, 94.8(9)%*
$(D_3O)Fe_{3-x}Al_y(SO_4)_2(OD)_6$	3.8D, 30.7 Fe, <0.9 Al, 13.2 S, 51.4 O	$Fe_{2.67}Al_{0.15}D_{9.2}S_{2.00}O_{15.58}$	89±3%
$NaFe_3(SO_4)_2(OD)_6$	3.5 D, 32.9 Fe, 13.2 S, 2.8 Na, 47.6 O	$Fe_{2.86}Na_{0.59}D_{8.50}S_{2.00}O_{14.5}$	95±4%
$(ND_4)Fe_3(SO_4)_2(OD)_6$	4.4 D, 32.9 Fe, 13.8 S, 2.0 N, 46.9 O	$Fe_{2.74}N_{0.66}D_{10.23}S_{2.00}O_{13.63}$	91±3%
$AgFe_3(SO_4)_2(OD)_6$	2.6 D, 27.2 Fe, 11.6 S, 6.0 Ag, 52.6 O	$Fe_{2.68}Ag_{0.31}D_{14.44}S_{2.00}O_{18.12}$	89±3%
$RbFe_3(SO_4)_2(OD)_6$	3.1 D, 28.3 Fe, 12.4 S, 9.4 Rb, 46.8 O	$Fe_{2.62}Rb_{0.57}D_{8.02}S_{2.00}O_{15.13}$	87±3%

and in previous experiments[49–51] are displayed in Table I. Any compositional data available from neutron diffraction has also been included.

Previous work has shown that a reduction in the reaction temperature reduces the iron content of the jarosite.[56,61] For this reason the synthesis of the site-diluted hydronium jarosite was carried out at the reduced temperature of 110 °C. $Al_2(SO_4)_3\,18H_2O$ was also introduced to reduce the partial iron concentration. Chemical analysis of the product did indeed show a reduced iron content (~89% occupation). The trace amount of aluminum incorporated into the structure indicates a large degree of preferential incorporation of iron under these conditions. The iron vacancies are thus charge balanced by protonation of hydroxy groups. The partially deuterated $(D_3O)Fe_{3-x}Al_y(SO_4)_2(OD)_6$ was prepared by dissolving 20.000 g of $Fe_2(SO_4)_2\,nH_2O$ and 31.500 g $Al_2(SO_4)_3\,18H_2O$ (Fisons 98%) in 50 ml D_2O with gentle heating and then most of the water was removed by rotary evaporation; the viscous fluid that remained was made up to 300 ml in D_2O and heated at 110 °C for 24 h, yielding 0.12 g of product. This material is a lighter shade of ochre than the pure iron compound.

B. Magnetic susceptibility measurements

dc susceptibility measurements were performed with a Quantum Design $MPMS_2$ SQUID magnetometer. Samples were held in gelatine capsules which had a small diamagnetic signal, and the magnetization was measured as a function of field at both low ($<T_f$) and high (≅300 K) temperatures to see if there was any evidence for ferromagnetic impurities or other forms of extrinsic magnetism.[48] The magnetization was then determined in a number of measuring fields between 10 and 10 000 Oe for temperatures between 1.8 and 350 K. Data were taken both under field-cooled and zero-field-cooled conditions to determine whether χ_{dc} in the region of T_f bore any evidence for spin glass freezing, and in all cases data were corrected for the diamagnetism of the sample holder and the constituent atoms.

C. Powder neutron diffraction

Neutron diffraction patterns were taken for deuterated forms of all the samples using a variety of diffractometers. Samples were held in a vanadium can and data were taken above and below T_f except for the rubidium salt which was only measured below T_f.

The sodium jarosite sample was measured on the POLARIS diffractometer of the ISIS Facility at temperatures of 40, 50, and 300 K using 8 g of sample. The nuclear and magnetic structure were refined from the 40 K data set collected over 11 h (1800 μA h) using both the *A* (low-angle) and *C* (high-angle) detector banks. A weak Bragg reflection was observed at $d=2.13$ Å and attributed to the vanadium sample can; data in this region of the pattern were excluded from subsequent profile refinement. The ammonium jarosite sample was measured on the D2B diffractometer at the Institut Laue-Langevin at a wavelength of 1.5943 Å with the (115) reflection of germanium as the monochromator. Data were taken from a 14 g sample at temperatures of 1.5 and 60

TABLE II. Magnetic parameters for pure and dilute jarosites derived from dc susceptibility and powder neutron diffraction data: T_f is the temperature of the cusp in the susceptibility, *C* is the gradient of the inverse susceptibility plotted against temperature for the linear region and θ is the intercept of this line with the temperature axis; μ_{eff} and *J* are the effective moment and exchange constant derived from *C* and θ, respectively. Note that the sublattice magnetization m_s was measured at different temperatures for different samples (40 K for the sodium salt, 1.4 K for the Fe/Al sample, and 1.5 K for the rest). *x* is the coverage of the magnetic lattice and all quantities have been normalized to this where appropriate.

Material	T_f/K	θ/K	*C*/emu mol^{-1}K^{-1}	μ_{eff}/μ_B	*J*/K	m/μ_B	*x*
$NaFe_3(SO_4)_2(OD)_6$	42,62	−667(5)	5.65(4)	7.13(3)	38.1(4)	2.07(4)	0.95
$(ND_4)Fe_3(SO_4)_2(OD)_6$	46,62	−640(5)	5.57(5)	7.08(3)	36.6(3)	4.38(11)	0.91
$AgFe_3(SO_4)_2(OD)_6$	51	−677(4)	5.70(5)	7.16(3)	38.7(4)	3.24(10)	0.89
$RbFe_3(SO_4)_2(OD)_6$	47	−688(5)	5.74(5)	7.19(3)	39.3(3)	2.74(7)	0.87
$(D_3O)Fe_{3-x}Al_y(SO_4)_2(OD)_6$	25.5	−720(5)	5.91(7)	7.29(5)	41.1(3)	1.44(9)	0.89

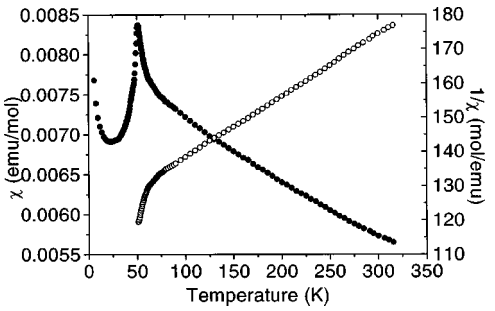

FIG. 5. (●) Field-cooled dc susceptibility and (○) inverse susceptibility of $AgFe_3(SO_4)_2(OD)_6$ as a function of temperature.

K. The rest of the samples (argento, rubidium and the aluminum-doped deuteronium jarosite) were measured on the D1B diffractometer at the Institut Laue-Langevin at a wavelength of 2.52 Å using the (002) reflection of pyrolytic graphite as the monochromator. Patterns for argentojarosite were taken on a 1.2 g sample at 1.5 K and 65.0 K; for rubidium jarosite a pattern was collected from ~2.8 g of sample at 1.5 K; for $(D_3O)Fe_{3-x}Al_y(SO_4)_2(OD)_6$ diffraction patterns were taken at 1.4 and 30.8 K from ~0.1 g of sample.

III. RESULTS

A. dc susceptibility

All members of the jarosite series other than the hydronium or deuteronium salts behave in a similar fashion with a linear dependence of the magnetization M with applied field H over the range 0 to 10 000 Oe. All samples display a cusp in χ_{dc} at a temperature of the order of 50 K and there is no significant divergence in the field-cooled and zero-field-cooled susceptibility. In all cases the inverse susceptibility is linear in temperature from approximately 150 K to the maximum experimental temperature of 350 K, and a fit to the Curie Weiss Law in this region yields a Weiss constant θ of the order of -700 K and a slope of the order of 5.5 emu mol^{-1} K^{-1}; exact values for C and θ for each compound are given in Table II. Figure 5 depicts the change in the susceptibility and in the inverse susceptibility with temperature for the silver salt, a measurement typical of all the undoped materials reported here, while Fig. 6 expands the susceptibility data in the region of T_c for each material. We note in passing that in some cases, notably that of the rubidium salt, the freezing transition is single, while in others there may be evidence of other transitions; we return to this point and a discussion of these data in greater detail in Sec. IV. In contrast to the data for the pure compounds, measurements on deuteronium jarosite doped with aluminum showed a freezing transition at 25.5 K but no further anomalies down to 1.8 K. Data for this sample are reproduced in Fig. 7.

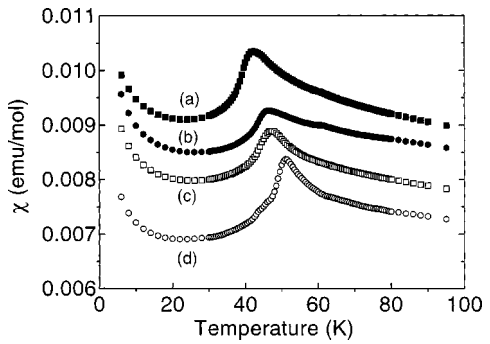

FIG. 6. Susceptibility of $AFe_3(OH)_6(SO_4)_2$ measured in an applied field of 10 000 Oe in the region of T_f for (a) A=Na, (b) ND_4, (c) Rb, and (d) Ag. Data have been offset by successive increments of 0.0005 emu mol^{-1} between neighboring datasets going up the page.

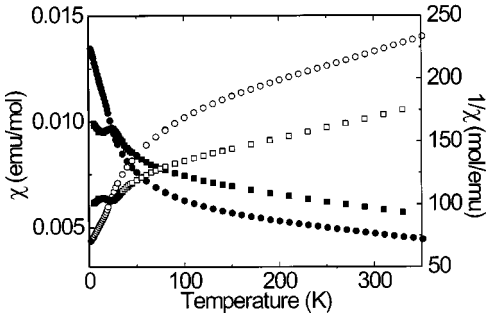

FIG. 7. Zero-field-cooled susceptibility and inverse susceptibility of $(D_3O)Fe_{3-x}Al_x(SO_4)_2(OD)_6$ and $(D_3O)Fe_3(SO_4)_2(OD)_6$ as a function of temperature, measured in 10 000 Oe field. Blocked-in symbols represent the susceptibility, and open symbols the inverse susceptibility, while circles and squares represent data for the doped and undoped material, respectively.

B. Powder neutron diffraction

The powder neutron diffraction pattern of sodium jarosite taken on the POLARIS diffractometer at 50 K showed no evidence of magnetic long-range order; however, diffuse scattering of the form observed in hydronium jarosite was seen,[50,54] though the flux distribution of this diffractometer is such that the signal is very weak over this range of d spacing. On cooling below the magnetic freezing temperature of this compound ($T_f \cong 42$ K) to 40 K, additional Bragg peaks were observed which were attributed to long-range magnetic order and indexed successfully on the basis of the magnetic unit cell assigned to $KFe_3(SO_4)_2(OD)_6$,[52] i.e., the in-plane spin structure corresponded to the $q=0$ array, and relative orientation of the in-plane component of the moments of nearest interlayer neighbors is 60°, leading to a doubling of the c axis relative to the nuclear unit cell. The relative orientations of moments in successive layers is given in Fig. 8(a); an alternative spin structure in which nearest-neighbors in adjacent layers are correlated antiferromagnetically (120°) is

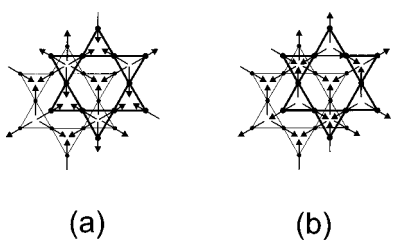

FIG. 8. Spin orientations for the $q=0$ spin structure in successive *kagomé* layers stacked along the c-axis of a jarosite when the nearest-neighbor interlayer correlations are predominantly (a) ferromagnetic and (b) antiferromagnetic.

TABLE III. Structural parameters for $NaFe_3(SO_4)_2(OD)_6$ at 40 K in the space group $R\bar{3}m$ with $Z=3$. Figures with asterisks are reported without errors because they were subject to rigid body constraints or their values fixed. Nuclear cell parameters: $a=7.32582(6)$ Å, $c=16.59516(20)$ Å; $R_{wp}=1.87\%$ (A bank), 2.67% (C bank), 2.47% (combined data set). $R_p=1.41\%$ (A bank), 2.68% (C bank), 1.86% (combined data set). Sublattice moment: 2..07 (4) μ_B.

Atom (Wyckoff site)	x	y	z	U_{iso}/Å^2	Site symmetry	Fractional occupancy
Fe (9d)	0.16667	−0.16667	−0.16667	0.0108(4)	2/M(110)	0.95(*)
S (6c)	0.00000	0.00000	0.30695(27)	0.0111(9)	3M(100)	1.000
O1 (6c)	0.00000	0.00000	0.39721(15)	0.0158(4)	3M(100)	1.000
O2 (18h)	0.22355 (9)	−0.22355 (9)	−0.05283 (7)	0.0158(4)	M(110)	1.000
O3 (18h)	0.12621(12)	−0.12621(12)	0.13362 (8)	0.0143(5)	M(110)	1.000
Na (3a)	0.00000	0.00000	0.00000	0.052 (4)	−3M(100)	0.585(*)
O4 (6c)	0.00000	0.00000	−0.02611(66)	0.0076(*)	3M(100)	0.208(*)
D1 (18h)	−0.07243(*)	0.07243(*)	−0.04284(66)	0.2840(*)	M(110)	0.208(*)
D4 (18h)	0.19566(12)	−0.19566(12)	0.10790(10)	0.0322(6)	M(110)	1.000

shown in Fig. 8(b). This second spin structure is observed in chromium analogues of the jarosites[28,52] and we will discuss the preference for the two spin structures in Sec. IV. The nuclear and magnetic structures were refined simultaneously from the A and C bank data collected at 40 K using the software package GSAS (Ref. 62) and starting from the $R\bar{3}m$ cell of hydronium jarosite. There was no evidence of crystalline impurity phases.

The 12 coordinate cavity in the sulfate layers may be occupied by both Na^+ and D_3O^+ ions. We assumed a random distribution of these ions, and constrained the D_3O^+ unit to be rigid with the same configuration as the hydronium ion in the pure hydronium salt. The refinement diverged if the fractional occupancy or thermal parameters of the Na^+ or the D_3O^+ ions was allowed to vary in an unconstrained fashion; consequently the thermal parameters of the D_3O^+ unit were fixed at the values refined for $(D_3O)Fe_3(SO_4)_2(OD)_6$ (Ref. 51) and the Na^+ and D_3O^+ fractional occupancies were set at those obtained from chemical analysis. The Fe occupancy and the thermal parameters failed to refine freely so the fractional occupation was also set at the value determined by chemical analysis. The uncertainty in the degree of isotopic substitution was treated by altering manually the scattering length of the D atoms until its occupation refined to 1.0 and this procedure was repeated for the remaining partially deuterated samples. The thermal parameters of the sulfate oxygen atoms were constrained to be the same as each other. Nuclear structural parameters are given in Table III.

The magnetic structure of sodium jarosite at 40 K was refined using data from just the A bank; a fault in the refinement program prevented the simultaneous use of both the A and C bank data for the magnetic refinement. The magnetic refinement is not affected greatly by this as the form factor of the magnetic scattering reduces its intensity considerably over the range of d spacing received by the C bank detector. Magnetic Bragg peaks in the C bank data were not excluded from the refinement because we wished to display them in the refinement profile, so the values for R_{wp} and R_p will be inflated relative to the value expected for the nuclear refinement alone. Previous work[28,52] suggested that magnetic order propagates along the c axis such that the order in successive kagome layers adopts the sequence $\cdots ABC-A-B-C\cdots$, where A, B, and C denote a $q=0$ array with different principal axes, and the negative sign a reversal of those axes. The magnetic unit cell is then twice as large as the nuclear unit cell along the c axis and can be described using $P\bar{3}$ symmetry. This spin structure was refined, yielding the magnetic propagation vectors given in Table IV and a sublattice magnetization of 2.07(4) μ_B, approximately 41% of the saturation value of $S=\frac{5}{2}Fe^{3+}$. It should be noted that the value of (T/T_f) is close to 1.0 so we anticipate that the saturated value of the sublattice magnetization is appreciably larger. The refined profiles for $NaFe_3(SO_4)_2(OD)_6$ are displayed in Fig. 9.

Nuclear structures of all the other samples were refined in a similar manner, though in the case of the ammonium salt, additional constraints had to be imposed on the refinement: the ND_4^+ ion was defined was a rigid unit with a bond length of 1.03 Å.[63] Data for this salt were taken on the diffractometer D2B, which has a very high resolution and this introduced further complications as we were unable to model the profile function with particular success. This is reflected in the poor values of R_{wp} and χ^2 and the unstable thermal parameters given in Table V. The physical origin of this could be a slight structural distortion away from the $R\bar{3}m$ space group or the presence of an impurity phase with a similar structure. This is to be expected because for many years there has been an argument as to whether the natural minerals belong to a noncentrosymmetric space group rather than $R\bar{3}m$ due to the observation of pyroelectricity.[64] If present, this distortion is very small as our attempts to model

TABLE IV. Positional parameters of iron atoms and magnetic unit vectors refined in the space group $P\bar{3}$ in $NaFe_3(SO_4)_2(OD)_6$ and applicable to the other jarosites in this work.

Atom	x	y	z	m_x	m_y	m_z
Fe (1)	0.5	0.5	0.75	−0.8667	0.5000	0.0000
Fe (2)	0.6667	0.8333	0.4167	0.8667	0.5000	0.0000
Fe (3)	0.8333	0.6667	0.0833	0.0000	−1.0000	0.0000

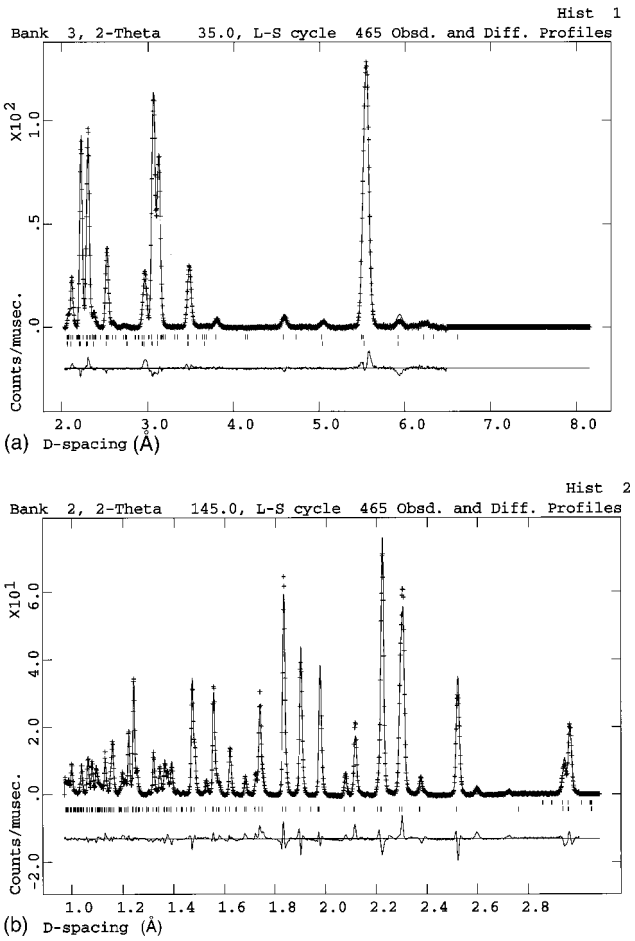

FIG. 9. Neutron-diffraction data for $NaFe_3(SO_4)_2(OD)_6$ taken on (a) the *A* bank (low-angle) and (b) the *C* (high-angle) detector bank of the POLARIS diffractometer at 40 K showing a fit to the $R\bar{3}m$ nuclear (lower ticks) and $P\bar{3}$ magnetic (upper ticks) unit cells and the difference between the data and fitted profile on the same scale (lower trace on each figure). $R_{wp}=1.87\%$ (*A* bank), 2.67% (*C* bank), 2.47% (combined data set). $R_p=1.41\%$ (*A* bank), 2.68% (*C* bank), 1.86% (combined data set).

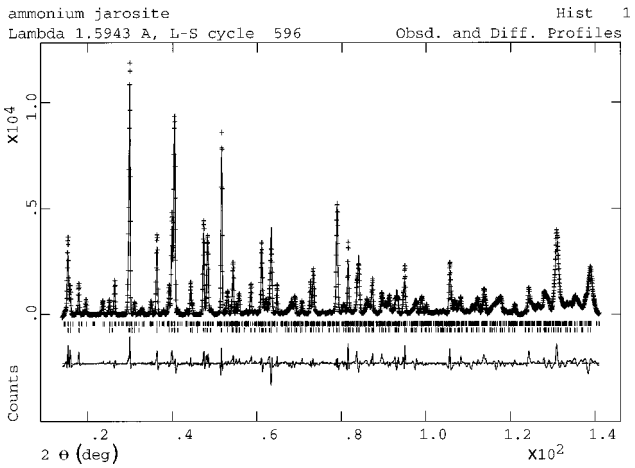

FIG. 10. Neutron-diffraction data for $(ND_4)Fe_3(SO_4)_2(OD)_6$ taken on the diffractometer D2B at 1.5 K showing a fit to the $R\bar{3}m$ nuclear (lower ticks) and $P\bar{3}$ magnetic (upper ticks) unit cells and the difference between the data and fitted profile on the same scale (lower trace). $R_{wp}=10.4\%$. $R_p=7.46\%$.

it by reducing the symmetry to the maximal nonisomorphic subgroups of $R\bar{3}m$, failed to lead to an improvement in the description of the lineshape. Refined structural parameters for the ammonium salt are given in Table V and the fitted profile displayed in Fig. 10.

The diffractometer D1B is a relatively high flux instrument that is particularly suitable for measuring Bragg reflections at long *d* spacing, but does not extend to sufficiently short *d* spacings to perform high quality nuclear structural refinements. However, the instrument is very suitable for measuring the diffuse scattering that we have attributed to short-range magnetic correlations in these compounds. Profile refinements of the nuclear structure were performed for argento-, rubidium-, and aluminum-doped deuteronium iron jarosite, but only to provide an estimate of the cell parameters and a detailed background for fitting of the diffuse scattering and the magnetic Bragg peaks. A summary of some of the nuclear structural data for these and the other compounds

TABLE V. Structural parameters for $(ND_4)Fe_3(SO_4)_2(OD)_6$ at 1.5 K in the space group $R\bar{3}m$ with $Z=3$. Figures with asterisks are reported without errors because they were subject to rigid body constraints or their values fixed. Nuclear cell parameters: $a=7.32877\,(32)$ Å and $c=17.3024\,(8)$ Å. $R_{wp}=9.9\%$, $R_p=7.46\%$. Sublattice moment: $4.38\,(11)\,\mu_B$.

Atom (Wyckoff site)	*x*	*y*	*z*	$U_{iso}/Å^2$	Site symmetry	Fractional occupancy
Fe (9*d*)	0.16667	−0.16667	−0.16667	0.0001 (7)	2/M(110)	0.910
S (6*c*)	0.00000	0.00000	0.3039 (12)	0.031 (4)	3M(100)	1.000
O1 (6*c*)	0.00000	0.00000	0.38983(40)	0.0088 (9)	3M(100)	1.000
O2 (18*h*)	0.22338(28)	−0.22338(28)	−0.05658(20)	0.0088 (9)	M(110)	1.000
O3 (18*h*)	0.12959(27)	−0.12959(27)	0.13598(25)	0.01 (9)	M(110)	1.000
O4 (6*c*)	0.00000	0.00000	−0.00565(73)	0.0076 (*)	3M(100)	0.170
D1 (18*h*)	−0.072403 (*)	0.072403 (*)	−0.02169(86)	0.2840 (*)	M(110)	0.170
N (6*c*)	0.00000	0.00000	−0.0097 (9)	0.022 (4)	3M(100)	0.330
D (18*h*)	−0.0745 (*)	0.0745 (*)	−0.02896(86)	0.1540(174)	M(110)	0.330
D (6*c*)	0.00000	0.00000	0.04810(86)	0.1540(174)	3M(100)	0.330
D4 (18*h*)	0.19621(28)	−0.19621(28)	0.10815(21)	0.0175 (10)	M(110)	1.000

TABLE VI. Summary of structural data for jarosites, both from this work and reported elsewhere (Refs. 37,49,51). The distances Fe-Fe, Fe-O(n), and the angle α [Fe(1)-O(1)-Fe(2)] refer to the nearest-neighbor iron atoms and the oxygen atoms to which they are bound, with $n=1$ or 2 defined in Fig. 15; H-O is the H(D)-bonding distance between hydroxide units and sulfate, and the angle β is between D(1)-O(3)-D(2) and is also defined in Fig. 15. Data for the rubidium-, argento-, and aluminum-doped deuteronium salt are less extensive because the data set taken on diffractometer D1B was not suitable for detailed structural refinement.

Material (Temperature)	a/Å	c/Å	Fe-Fe /Å	Fe-O(1) /Å	Fe-O(2) /Å	H-O /Å	α/°	β/°
$(H_3O)Fe_3(SO_4)_2(OH)_6$ (1.5 K) (Ref. 49)	7.32457(12)	16.9153(4)	3.66228(6)	2.0374(9)	1.9921(8)	1.946	133.625	106.1
$(D_3O)Fe_3(SO_4)_2(OD)_6$ (2.0 K) (Refs. 49,50)	7.3445(7)	16.9037(16)	3.6722(3)	2.013(4)	1.9908(20)	1.908	134.53(27)	105.5
$(D_3O)Fe_{3-x}Al_x(SO_4)_2(OD)_6$ (1.4 K)	7.3399(6)	16.9897(31)						
$NaFe_3(SO_4)_2(OD)_6$ (40 K)	7.32582(6)	16.59516(20)	3.6629(6)	2.0222(2)	1.9878(2)	1.893	134.248(12)	106.1
$KFe_3(SO_4)_2(OH)_6$ (10 K) (Ref. 37)	7.30	17.09	3.65				134	
$(ND_4)Fe_3(SO_4)_2(OD)_6$ (1.5 K)	7.32877(32)	17.3024(8)	3.66415(19)	2.036(4)	1.9939(15)	1.962	133.51	101.0
$RbFe_3(SO_4)_2(OD)_6$ (1.5 K)	7.3342(9)	17.3884(29)						
$AgFe_3(SO_4)_2(OD)_6$ (1.5 K)	7.3573(12)	16.5242(28)						

in this work is given in Table VI, and fitted profiles are displayed in Figs. 11–13.

The broad asymmetric peak was fitted to a Warren function[50,65–67] which was originally developed[65] to describe diffuse scattering of x rays from graphite, a material in which there is long-range structural order within a set of planes, but no structural correlations between these planes. The structure factor for a particular reflection from one of these two-dimensional objects corresponds to a rod in reciprocal space centered at the indices (h,k) of the reflection. Thus, as a powder diffraction pattern is measured with increasing scattering vector, such a reflection will produce a sharp rise in the scattering intensity when $Q=Q_0=ha^*+kb^*$, where a^* and b^* are reciprocal lattice vectors for the unit cell. As Q continues to increase, the Ewald sphere continues to cut the rods of scattering, and the scattering strength per unit of Q, P_Q, falls gradually with Q as the scattering is distributed over an increasing solid angle. In real materials, the two-dimensional objects will have a finite width L, which broadens the rods of scattering and consequently broadens P_Q, as well as shifts the maximum by an amount $\Delta Q=0.64\pi/L$, where λ is the wavelength of the radiation. Such a model has been adapted[66,67] to describe the diffuse scattering from a layered magnet in which there are short-range correlations of length L within a plane, but no correlation between them. P_Q may be expressed as

$$P_Q = KmF_{hk}^2[2Q(\lambda/4\pi)+Q^{-1/2}(\lambda/4\pi)^{-2}-2] \times\left(\frac{QL}{4\pi^{3/2}}\right)^{1/2} F(a)[J(Q)]^2, \quad (2)$$

where K is a scaling constant, m is the multiplicity of the reflection, F_{hk} is the two-dimensional structure factor for the spin array and $J(Q)$ is the magnetic form factor. The function $F(a)$ describes the way in which the Ewald sphere cuts through the rods of scattering as Q increases, and is calculated by integration in cylindrical coordinates over a range of scattering vectors centred at Q_0 for the (hk) reflection, such that the angle between Q and Q_0 is φ. For small φ, $F(a)$ is given by

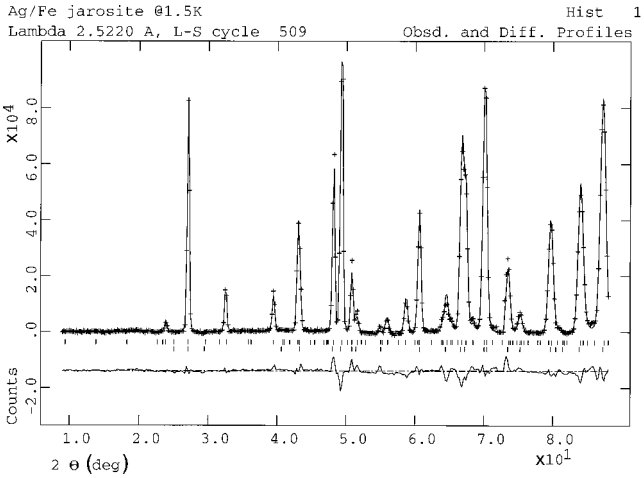

FIG. 11. Neutron-diffraction data for $AgFe_3(SO_4)_2(OD)_6$ taken on the diffractometer D1B at 1.5 K showing a fit to the $R\bar{3}m$ nuclear (lower ticks) and $P\bar{3}$ magnetic (upper ticks) unit cells and the difference between the data and fitted profile on the same scale (lower trace). $R_{wp}=3.16\%$. $R_p=2.33\%$.

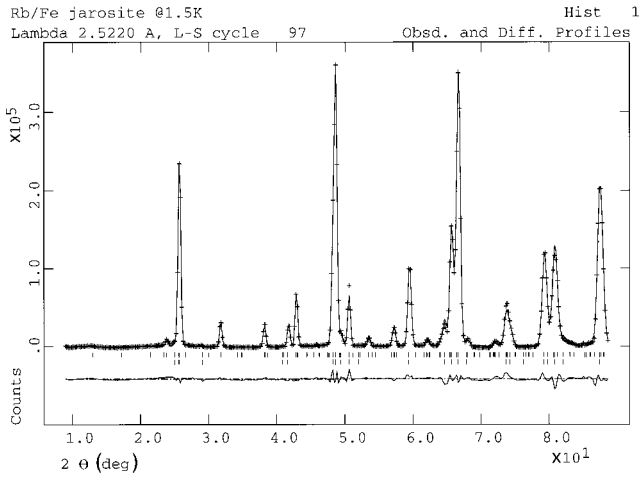

FIG. 12. Neutron-diffraction data for $RbFe_3(SO_4)_2(OD)_6$ taken on the diffractometer D1B at 1.5 K showing a fit to the $R\bar{3}m$ nuclear (lower ticks) and $P\bar{3}$ magnetic (upper ticks) unit cells and the difference between the data and fitted profile on the same scale (lower trace). $R_{wp}=3.36\%$. $R_p=2.53\%$.

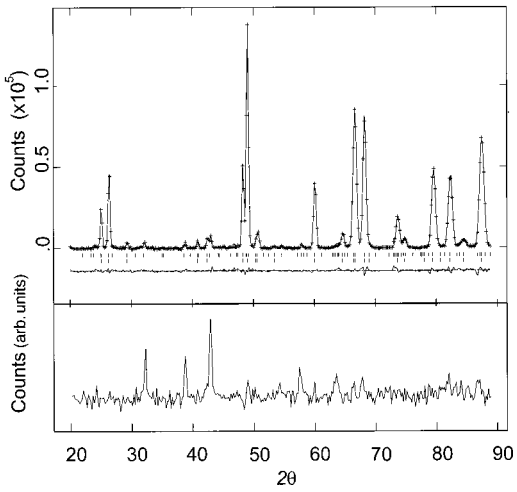

FIG. 13. Neutron-diffraction data for $(D_3O)Fe_{3-x}Al_x(SO_4)_2(OD)_6$ taken on the diffractometer D1B at 1.4 K showing a fit to the $R\bar{3}m$ nuclear (lower ticks) and $P\bar{3}$ magnetic (upper ticks) unit cells and the difference between the data and fitted profile on the same scale (lower trace). $R_{wp}=1.16\%$. $R_p=0.85\%$. The data at the bottom of the figure represent the difference between patterns taken at 30.8 and 1.4 K, multiplied by a factor of 12 to make it easier to identify what appear to be magnetic Bragg peaks.

$$F(a)=\int_0^\infty \exp[-(x^2-a)^2]dx, \tag{3}$$

where

$$a=\left(\frac{L}{2\sqrt{\pi}}\right)(Q-Q_0) \tag{4}$$

and

$$x=\varphi\left(\frac{LQ}{4\sqrt{\pi}}\right). \tag{5}$$

While the integral in Eq. (3) was originally given in Warren's work as being over the limits 0 to ∞, it does not converge and in practice is calculated between finite limits; we found the values 0 to 10 produced no significant difference relative to the values tabulated in Warren's original article.

The expression for P_Q was fitted to data for ammonium-, rubidium-, argento-, and aluminum-doped hydronium iron jarosite at a number of different temperatures to give the spin-spin correlation lengths detailed in Table VII. An example of such a fit for the argentojarosite data is given in Fig. 14. In addition, all the diffraction patterns taken below T_f for these materials showed additional Bragg peaks that could be indexed and refined in the same manner as for the sodium salt. Refined values for the ordered moments of these materials are also given in Table II. Remarkably, the aluminum-doped hydronium jarosite does show additional Bragg peaks below T_f in contrast to the undiluted salt which only shows a Warren peak at temperatures well below T_f. The diffraction pattern of 0.1 g of $(D_3O)Fe_{3-x}Al_x(SO_4)_2(OD)_6$ was taken at 30.8 and 1.4 K and showed additional Bragg peaks at the lower temperature which could be refined to the same $P\bar{3}$ spin array with a saturated moment of $1.44(9)\mu_B$ ($R_{wp}=1.16\%$ and $R_p=0.85\%$) (Fig. 13). We also observed diffuse magnetic scattering at both temperatures which resembled that observed in the undoped materials, and this part of the pattern was also fitted to a Warren function with an in-plane spin-spin correlation length $\xi=16.2\pm2.5$ Å.

TABLE VII. Summary of parameters for fits of a Warren function to the diffuse magnetic scattering observed at low temperatures in jarosites.

A cation	*T*/K	*L*/Å	Q_0/Å^{-1}
D_3O (Ref. 50)	60	15 ± 4	1.02
D_3O(Fe/Al)	30.8	16.2 ± 2.5	1.06
Na			
ND_4	60	19.1 ± 0.1	1.02
ND_4	1.5	15 ± 4.0	1.02
Ag	65	18.5 ± 0.8	1.05
Ag	1.5	18.7 ± 2.2	1.05
Rb	1.5	22.5 ± 4	1.01

In principle, the value of Q_0 should provide information about the nature of the in-plane spin-array, corresponding to indices for dominant reflections. The spread of values we observe for Q_0, in the range $1-1.15$ Å^{-1}, are compatible with the results of Monte Carlo simulation for the nearest-neighbor *kagomé* Heisenberg antiferromagnet,[14] and also with exact analysis of the infinite component *kagomé* antiferromagnet,[68] which predict maxima in $S(Q)$ at approximately 1.15 and 1.0 Å^{-1}, respectively, for a cell with the dimensions of the compounds reported here.

IV. DISCUSSION

The principal result of this work is the observation that jarosites appear to be divided into two categories according to the nature of the magnetic correlations in the low-temperature frozen state. All jarosites studied to date[37,42–48,52] with the exception of the hydronium or deuteronium salt[49,50] show long-range magnetic order with the $q=0$ structure in the *kagomé* layers, and in the case of Fe^{3+} salts the magnetic unit cell is doubled along the *c* axis com-

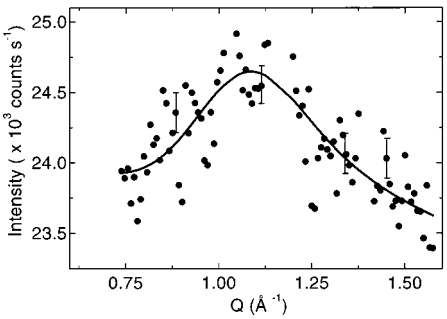

FIG. 14. Diffuse scattering peak indicative or short-range antiferromagnetic order in the *kagomé* layers of argentojarosite observed at 1.5 K. The solid line through the data is the least-squares fit to a Warren function. The gaps in the data are regions where there are the strong nuclear reflections, and these were removed for the purposes of the fit.

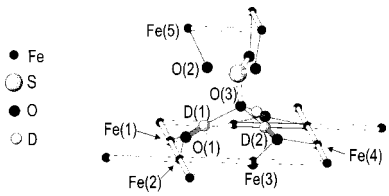

FIG. 15. Exchange pathways in the jarosite structure. The figure depicts fragments of two neighboring *kagomé* planes of iron atoms. Within such planes an iron atom (1) may interact with second (3) and third-nearest neighbors (4) through hydrogen-bonded interactions between hydroxy and sulfate groups (dotted lines), as well as by strong superexchange with nearest neighbors (2) through a covalent bond [O(1)]; exchange with an atom (5) in a neighboring plane may also propagate through hydrogen-bonded interactions involving the sulfate group.

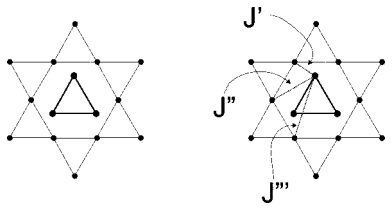

FIG. 16. Definition of further-neighbor interlayer exchange interactions in the jarosite structure J', J'', and J''' are first, second, and third neighbor exchange interactions ranked according to shortest through-space distance between iron atoms.

pared to the nuclear unit cell (the exception is the potassium analogue in which sulfate is exchanged for chromate for which the magnetic and nuclear unit cells have the same c parameter[50]). In all cases where long-range magnetic order is observed, freezing sets in around 50 K. Further, those chromium isomorphs that have been studied (where Cr is substituted for Fe) also show long-range magnetic order at low temperature,[28] with the $q=0$ structure in the kagome layers and a nondoubled c axis. The spin arrays in the single- and doubled-magnetic unit cells for in-plane $q=0$ correlations have been displayed schematically in Figs. 8(a) and 8(b), revealing the relative spin orientations between layers. It can be seen that the doubled unit cell arises when the nearest-neighbor interlayer magnetic correlations have a ferromagnetic component with relative orientation of in-plane components of 60°, while the single-c magnetic cell corresponds to 120° antiferromagnetic nearest-neighbor interlayer correlations.

In order to rationalize the various spin arrays that may form it is necessary to consider the nature of the exchange pathways in these compounds in more detail. There are no data available for the relative strengths of further neighbor exchange either within or between the *kagomé* layers in any of these compounds, and it is unlikely that any unambiguous data will be available until careful spin-wave dispersion measurements have been performed on single crystals of these materials. Instead, we will consider what pathways are likely to be significant on the basis of exchange geometry so that we can judge what the most important perturbations to the simple Hamiltonian (2) for nearest-neighbor Heisenberg exchange are likely to be; such interactions have already been considered for potassium jarosite, but at that time the location of the hydrogen atoms in the structure was not known and these may be important for a thorough analysis.[43]

In jarosites the nearest-neighbor in-plane exchange J propagates through shared oxygen atoms provided by the hydroxide molecules of the coordination octahedra of Fe^{3+} (Figs. 3, 4, 15). Further-neighbor in-plane exchange may pass through the same hydroxide groups which are hydrogen bonded to the apical oxygen atom of the sulfate group. There is considerable evidence for efficient exchange through H-bonded atoms in other materials.[69,70] Such pathways, illustrated in Fig. 15, are likely to be of comparable strength for second and third-neighbor in-plane exchange J_2 and J_3, respectively; the path length for both exchange routes is identical, the difference being in the bonding angle between H atoms and apical oxygen. If this route is viable for further-neighbor in-plane exchange, it should also provide part of the pathway for an interlayer exchange of comparable strength. It is known that the sulfate group may provide an efficient exchange pathway in a variety of transition metal compounds,[71] so any spin polarization transferred from Fe^{3+} to the apical sulphur atoms may also be passed up to Fe^{3+} ions in the neighboring layer. This provides three different types of interlayer exchange which we will label J', J'', and J''', according to the through-space distance between the ions involved. Figure 16 depicts the various exchange interactions schematically as if they propagated through space, but we must remember *that the exchange pathways are made up of bonds through atoms and molecules* (Fig. 15). Some bond lengths and angles for these and other exchange pathways are given in Table VI. To a first approximation we would expect the strengths of these exchange interactions to be similar because the path *length* along the connecting bonds is the same in each case. However, the *angles* involved in every link in the path are different, so strictly speaking the interactions between the atomic orbitals that make up the molecular orbitals for each pathway may be different and the spin polarization may therefore be propagated differently between the various interlayer neighbors. It is very likely that J', J'', and J''' are all antiferromagnetic, ferromagnetic superexchange in insulators requiring some form of orthogonal linkage and being very rare.[72] Thus, if we assume that all interlayer exchange is antiferromagnetic, we may draw up a simple relationship between J', J'', and J''' for the nearest-neighbor interlayer correlations to be either ferromagnetic or antiferromagnetic, as described in Figs. 8(a) and 8(b). For the predominantly ferromagnetic (60°) case and a doubled c axis in the magnetic cell, $|J''|>|(J'+J''')/2|$, and for the predominantly antiferromagnetic (120°) nearest-neighbor interlayer correlations, $|J''|<|(J'+J''')/2|$. It is quite possible that a change of Cr for Fe as the magnetic ion, or Cr for S in the exchange pathway, alters the relative values of J', J'', and J''' and tips the balance between single- and double-magnetic c axis. Fe and Cr have $3d^5$ and $3d^3$ valence electron configurations, respectively, which in a quasioctahedral environment become ${t_{2g}}^3{e_g}^2$ and ${t_{2g}}^3$, respectively, so it is likely that admixture of atomic orbitals from the metal atoms and the ligands in the exchange pathway are significantly different, giving rise to different relative values of J', J'', and J'''.

It has been pointed that the form of the exchange between layers may also influence the nature of the spin correlations within the *kagomé* layers.[28] Both ferromagnetic and antifer-

romagnetic interlayer coupling produce a net exchange field for the $q=0$ structure, but for the $\sqrt{3}\times\sqrt{3}$ spin structure, the $(\frac{2}{3}\frac{1}{3})$ in-plane translation between neighboring planes is out of registry with the periodicity of the order in the *kagomé* layers. Further-neighbor intralayer exchange, J_2 and J_3, is likely to be comparable in strength to J', J'', and J''' on the basis of the similarity in length and composition of the exchange pathways (Table VI) and this will also stabilize various forms of long-range order. Harris *et al.*[12] used linear spin-wave analysis to calculate how the energy of the $q=0$ and $\sqrt{3}\times\sqrt{3}$ spin structures changed when further-neighbor intralayer exchange was introduced and concluded that the $q=0$ structure was more stable when $(J_2-J_3)>0$, and the $\sqrt{3}\times\sqrt{3}$ spin structure was more stable when $(J_2-J_3)<0$. However, one should bear in mind that since these were the only spin structures considered, it is possible that the ground state spin array is different from either of these options.

If we assume that the exchange field is dominated by the nearest-neighbor in-plane exchange J, we may estimate the value of J from analysis of the high-temperature form of the susceptibility. In view of the relative lengths and compositions of the exchange pathways, this appears to be a reasonable assumption, but it should be noted that the neglect of further-neighbor interactions (assuming they are also antiferromagnetic) will overestimate the magnitude of $|J|$ by an amount $\Sigma_n zJ^nS(S+1)$, where z is the number of nth further neighbors. Recent series expansion calculations of the susceptibility of a *kagomé* antiferromagnet with the Hamiltonian of Eq. (1) (Refs. 12,14) indicate that although a conventional Curie-Weiss expression should describe the susceptibility well at high temperatures, a modified form will prevail below $T\cong JS(S+1)/k$. In this regime, the inverse susceptibility intercepts the temperature axis at $-2JS(S+1)/k$, rather than the value of $-(4/3k)JS(S+1)$ predicted by mean field theory, and its slope with temperature adopts a value $(\mu_{\rm eff})^2/9$ rather than the conventional value of $(\mu_{\rm eff})^2/8$, where $(\mu_{\rm eff})^2=g^2\mu_B^2S(S+1)$. Over the entire temperature range where the measured inverse susceptibility has a linear dependence on temperature, a single slope is observed, which suggests that all our measurements are in the lower temperature regime or below. The magnitude of $|J|$ derived from these data using the appropriate expression is of the order of 40 K in all cases, predicting that the transition from the low-to high-temperature susceptibility regime is at a temperature of the order of 350 K.

Applying this analysis to our susceptibility data we obtain effective moments that are significantly larger than the value expected for the ${}^6A_{1g}$ ground term of Fe^{3+} in this ligand field environment which should be free of either temperature independent paramagnetism or a second-order Zeeman effect, and should therefore adhere closely to the spin-only value of $\sqrt{35/4}\cong 5.92\mu_B$. It is possible that our samples contain a small amount of a ferromagnetic or ferrimagnetic impurity phase or that moments near inhomegeneities in the lattice are canted and produce a weak spontaneous magnetization. Anomalously high moments are observed by other workers.[48,53] Maegawa and co-workers[48] observed a nonlinear M vs H curve at low temperatures which was attributed to defect Fe^{3+} ions; the contribution from such impurities saturates in higher fields. It was observed that an applied field of 20–30 kOe was required for saturation of the magnetization in samples of sodium, potassium, and ammonium jarosite, and that substantial nonlinearity should be apparent below our maximum operating field of 10 kOe; we do not observe an indication of such behavior in our materials. Earle *et al.*[53] performed a careful study of the susceptibility of diamagnetically doped hydronium jarosite and concluded that the moment derived from the high-temperature susceptibility became higher as the lattice coverage increased, suggesting it was inherent to the kagome lattice as modelled by jarosites. This is turn could be attributed to approximations in the series expansion treatment of the susceptibility not treating the complexity of exchange interactions in jarosites sufficiently well.[53]

Some of our samples also show signs of a second magnetic transition at 61–62 K, not unlike the secondary transitions that have been observed in samples of sodium, potassium, and ammonium jarosite,[48,52] and which have been shown by NMR measurements to be inherent to these materials rather than a consequence of an impurity phase. This was interpreted as evidence for some form of intermediate magnetic phase. However, the fact that there is not an exact correspondence between data taken from different samples of the same materials suggests that the observation of this feature in measurements of $\chi_{\rm dc}$ may be influenced by the lattice coverage, which in turn is very sensitive to variations in the preparative conditions. We note that a transition above the main cusp in $\chi_{\rm dc}$ is most distinct in samples with the highest lattice coverage.

Precise values of the effective moment are given in Table II together with values for $|J|$, all of which are close to 40 K. There are relatively large changes in the cell parameter c and hence the interlayer separation as the A cation changes, but no consistent correlation between this and T_f or θ; changes in the cell parameter a, and hence the intralayer Fe-Fe separation are less marked, but again there is no clear, consistent relation with the magnetic parameters. The only parameter that appears to change steadily with the mass of the A-site cation is the coverage of the magnetic lattice; there is a less distinct trend in the variation of T_f with mass of the A-site cation, showing a noisy increase in T_f as the A cation gets heavier, and this could be related to the accompanying decrease in site coverage, although this is opposite to the conventional response of a magnet to dilution.

We find a similar, unconventional response to dilution when we consider the aluminum-doped hydronium jarosite. Apart from work on gallium-doped hydronium jarosite,[53] we are unaware of a *simple, insulating* system in which dilution leads to an increase in the temperature of spin freezing. T_f for SCGO(x) (Refs. 22,24) as well as for a chromium analogue of the jarosites,[28] falls with dilution [though it should be noted that this results pertains to *ceramic* samples of SCGO(x), while for *single crystals* grown from flux there is an apparent *increase* in T_f as site coverage increases,[20] a result that has been attributed to a preferential loss of magnetic ions from the *kagomé* sites in the structure as opposed to triangular lattice sites, and this in turn leads to a structure that is on average less two-dimensional]. There is relatively little theoretical work on the effect of magnetic inhomogeneities on kagome antiferromagnets. Shender and co-workers[10] deduced that the principal effect of varying the magnitude of spins on a *kagomé* antiferromagnet was to induce noncopla-

narity in the ground state; this work also predicted that the energy of any individual triangle would be minimized (except in the case of strong disorder where it is the energy of isolated clusters of moments that is minimized). The special case of site dilution (i.e., where the magnitude of the spin at a site is S or 0) has also been studied and indicates that the same rule for minimization of energy applies here too.[73] The rule of satisfied triangles or clusters suggests that dilution alone is unlikely to induce spin glass order: the fact that the ground state energy is independent of the separation of defects implies that the spin degrees of freedom of the defects do not couple. However, real model *kagomé* antiferromagnets such as the jarosites may differ because they have further-neighbor interactions, dipolar coupling and quantum fluctuations, so this problem requires further specific theoretical work. What is clear is that random dilution may create a local imbalance in exchange interactions near an impurity and may in some cases produce an increase in interlayer or intralayer exchange as a compensated triangle is disturbed. On average, this will lead to an overall reduction in the exchange field, and mean-field arguments would then predict a reduction in the temperature scale for any freezing. However, it is possible that higher-order effects operate, and local impurities pin down a longer-range spin structure. It has also been observed that T_f for hydronium *chromium* analogs *falls* on dilution of the magnetic sites[28,51] and this may reflect a different balance between exchange constants.

The sensitivity of the collective magnetic properties of jarosites towards the coverage of the magnetic lattice[53] might explain inconsistencies between measurements of materials which have the same nominal composition. We have observed that T_f varies from batch to batch of the same jarosite, so care should be taken in interpreting differences between magnetic parameters such as θ.

Powder neutron diffraction studies of the magnetic correlations in all of these materials reveal spin structures that are compatible both with observations in related materials, and with the predictions of theory, depending on further-neighbor exchange. At low temperatures the observed values of the sublattice magnetization are generally far below the $5.92\mu_B$ spin-only value expected for Fe^{3+}. In the case of the sodium salt this will be due in part to the relatively high temperature (40 K) of the measurement, but for the remaining salts, where measurements were made at 1.4 or 1.5 K, it is likely that this reflects loss of static long-range order to fluctuations or short-range static correlations, supported by the observation of the broad feature at lower temperatures which we fitted to the Warren function. Comparable reductions in ordered moment have been observed[28] in the $S=\frac{3}{2}$ *kagomé* antiferromagnet $KCr_3(OD)_6(SO_4)_2$, in which the ordered moment below T_f is approximately $\frac{1}{3}$ of the Néel value and this was attributed to gapless quantum spin fluctuations that persist down to at least 70 mK.

V. CONCLUSIONS

These measurements have shown that jarosites $AFe_3(OH)_6(SO_4)_2$ in which A^+ is Rb^+, ND_4^+, or Ag^+, all possess well-separated *kagomé* layers of Fe^{3+} ions with strong antiferromagnetic coupling. Above 100 K $1/\chi_{dc}$ is linear in temperature, providing an estimate of the Weiss constant θ of the order of -700 K in each case but yielding an estimate of the ordered moment that is anomalously high—of the order of $7\mu_B$—in each case as opposed to the value of $5.92\mu_B$ anticipated for a spin-only moment for $S=\frac{5}{2}$. In all cases a distinct cusp is observed in χ_{dc} at a temperature T_f of the order of 50 K. In some cases (Na^+ and ND_4^+ salts) additional, weak features are observed in the susceptibility above T_f, but they differ in location from similar features seen by other workers in these and other jarosites. Powder neutron diffraction provides detailed structural information for the Na and ND_4 salts, and also reveals that in every case the ordered spin structure below T_f corresponds to the $q=0$ spin array in the *kagomé* layers, and an antiferromagnetic arrangement between layers for which the magnetic unit cell is twice as large as the nuclear cell in the c direction. However, the ordered moment below T_f as deduced from the powder diffraction pattern, is less than 30% of the spin-only moment of Fe^{3+}, indicating that a large proportion of the moments are either fluctuating or possess short-range static correlations.

It is known that jarosites are prone to nonstoichiometry, losing Fe^{3+} from the lattice, and it is also anticipated that their magnetic properties are very sensitive to the coverage of the magnetic sublattice, so we advise caution in trying to compare properties of different materials and correlate structural and magnetic properties. A consideration of the relation between T_f and the lattice coverage implies that dilution leads to an *increase* in the freezing temperature. This counterintuitive result was confirmed for the case of the deuteronium salt which shows no long-range magnetic order down to 0.4 K, but rather a spin-glass-like transition at a temperature of the order of 15 K. On dilution with an aluminum isomorph, to produce, $(D_3O)Fe_{3-x}Al_y(OD)_6(SO_4)_2$, in which the coverage of the magnetic lattice is $89\pm3\%$, T_f was observed to rise to 25.5 K, and powder neutron diffraction measurements indicated that there was long-range magnetic order at 1.4 K. This result is not compatible with current theory for *kagomé* antiferromagnets for which dilution is only likely to reduce the temperature scale and lower any freezing transition. However, it is possible that further-neighbor exchange is significant in these materials and may give rise to net interlayer or intralayer exchange between uncompensated triangles of spins near vacancies which in turn selects a particular ground state. To investigate this effect further it is necessary to get a better estimate of further neighbor exchange interactions, which requires single crystals for detailed neutron scattering measurements of the spin waves. Laboratory growth of such crystals will be difficult, but it is probable that suitable samples exist in mineral collections. Complementary developments in theory are also required, to model the effect of magnetic inhomogeneities on magnetic correlations in such materials, and extend the current position between the somewhat idealized systems studied to date.

ACKNOWLEDGMENTS

We are grateful to EPSRC for financial support, and to both the ISIS Facility of the Rutherford Laboratory and to the Institut Laue-Langevin for technical support. A.H. is grateful to the Nuffield Foundation for financial support of some of this work. It is a pleasure to acknowledge a number

of people for stimulating and illuminating discussion of our measurements, and in particular we wish to thank Steve Bramwell, Collin Broholm, John Chalker, Michel Gingras, John Greedan, Peter Holdsworth, Thom Mason, and Art Ramirez.

APPENDIX

Here we give the details of the conditions used to synthesise the various jarosite samples studied in this paper. A partially deuterated sample of $NaFe_3(SO_4)_2(OD)_6$ was prepared by dissolving 51.600 g of $Fe_2(SO_4)_2\,nH_2O$ (Aldrich 97%) and 9.400 g Na_2SO_4 (Fisons 99%) in 300 ml D_2O.[59] The reaction solution was heated at 155 °C for 4 h. The mass of the final product was 12.48 g.

The literature synthesis[52] failed to yield an ammonium jarosite precipitate and instead resulted in the production of an amorphous species. A synthesis was designed using conditions derived from the preparation of $NaFe_3(SO_4)_2(OD)_6$. The partially deuterated sample was prepared by dissolving 51.600 g of $Fe_2(SO_4)_2\,nH_2O$ and 80.000 g $(NH_4)_2(SO_4)_3$ (Prolabo 99%) in 50 ml D_2O with gentle heating and reducing the reactant solution by rotary evaporation. The reactant was then made up to 300 ml with D_2O and heated at 155 °C for 4 h. The mass of the final product was 14.13 g.

The partially deuterated sample of $AgFe_3(SO_4)_2(OD)_6$ was prepared by mixing 6.000 g of $Fe_2(SO_4)_2\,nH_2O$ and 6.000 g Ag_2SO_4 (Aldrich 99.999%) in 50 ml D_2O with gentle heating (note that this amount of Ag_2SO_4 exceeds the solubility and so the Ag_2SO_4 will not completely dissolve).[52] The reactant solution was reduced by rotary evaporation before being made up to 200 ml with D_2O. 7.500 g D_2SO_4 (99.8 at. %, CDN Isotopes 96%) were added before the mixture was finally made up to 300 ml with D_2O. The reaction solution was heated at 155 °C for 4 h. The mass of the bright yellow product was 1.29 g. To minimize photodecomposition all silver-containing reagents, reaction solutions and products were handled under dull light conditions and their containers stored wrapped in aluminum foil.

The partially deuterated sample of $RbFe_3(SO_4)_2(OD)_6$ was prepared using a literature synthesis.[40] 46.500 g of $Fe_2(SO_4)_2\,nH_2O$ and 7.500 g Rb_2SO_4 (Fluka 98%) were dissolved in 50 ml D_2O with gentle heating and reducing the reactant solution by rotary evaporation. The reactant was then made up to 200 ml with D_2O and 4 drops of D_2SO_4 were added before the mixture was made up to 300 ml with D_2O. The reaction solution was heated at 111 °C for 4 h. The mass of the final product was 2.84 g.

*Present address: Centre D'Études Nucléaires de Grenoble, DRFMC/SPSMS/MDN, 17 Rue des Martyrs, 38054 Grenoble, Cédex 9, France.

†Author to whom correspondence should be addressed. Electronic address: a.harrison@ed.ac.uk

[1] G. Toulouse, Commun. Phys. **2**, 115 (1977).
[2] J. Villain, Z. Phys. **33**, 31 (1979).
[3] A. P. Ramirez, Annu. Rev. Mater. Sci. **24**, 453 (1994).
[4] M. F. Collins and O. A. Petrenko, Can. J. Phys. **75**, 605 (1997).
[5] H. Kawamura, J. Appl. Phys. **63**, 3086 (1988).
[6] B. D. Gaulin, in *Magnetic Systems With Competing Interactions (Frustrated Spin Systems)*, edited by H. T. Diep (World Scientific, Singapore, 1994), p. 286.
[7] M. L. Plumer, in *Magnetic Systems With Competing Interactions (Frustrated Spin Systems)* (Ref. 6).
[8] R. R. P. Singh and D. A. Huse, Phys. Rev. Lett. **68**, 1766 (1992).
[9] K. Yang, L. K. Warman, and S. M. Girvin, Phys. Rev. Lett. **70**, 2641 (1993).
[10] E. F. Shender, V. B. Cherepanov, P. C. W. Holdsworth, and A. J. Berlinsky, Phys. Rev. Lett. **70**, 3812 (1993).
[11] C. Zeng and V. Elser, Phys. Rev. B **42**, 8436 (1990).
[12] A. B. Harris, C. Kallin, and A. J. Berlinsky, Phys. Rev. B **45**, 2899 (1992).
[13] J. T. Chalker, P. C. W. Holdsworth, and E. F. Shender, Phys. Rev. Lett. **65**, 855 (1992).
[14] J. N. Reimers and A. J. Berlinsky, Phys. Rev. B **48**, 9539 (1993).
[15] A. Chubukov, Phys. Rev. Lett. **69**, 832 (1992).
[16] S. Sachdev, Phys. Rev. B **45**, 12 377 (1992).
[17] D. J. and C. L. Henley, Phys. Rev. B **48**, 965 (1993).
[18] D. Huse and A. Rutenberg, Phys. Rev. B **45**, 7536 (1992).
[19] X. Obradors, A. Labarta, A. Isalgué, J. Tejada, J. Rodriguez, and M. Pernet, Solid State Commun. **65**, 189 (1988).
[20] A. P. Ramirez, G. P. Espinosa, and A. S. Cooper, Phys. Rev. Lett. **64**, 2070 (1990).
[21] C. Broholm, G. Aeppli, G. P. Espinosa, and A. S. Cooper, Phys. Rev. Lett. **65**, 3173 (1990).
[22] A. P. Ramirez, J. Appl. Phys. **70**, 5952 (1991).
[23] A. P. Ramirez, G. P. Espinosa, and A. S. Cooper, Phys. Rev. B **45**, 2505 (1992).
[24] B. Martinez, F. Sandiumenge, A. Rouco, A. Labarta, J. Rodríguez-Carvajal, M. Tovar, M. T. Causa, S. Galí, and X. Obradors, Phys. Rev. B **46**, 10 786 (1992).
[25] P. Schiffer, A. P. Ramirez, K. N. Franklin and S. W. Cheong, Phys. Rev. Lett. **77**, 2085 (1996).
[26] S.-H. Lee, C. Broholm, G. Aeppli, T. G. Perring, B. Hessen, and A. Taylor, Phys. Rev. Lett. **76**, 4424 (1996).
[27] S.-H. Lee, C. Broholm, G. Aeppli, A. P. Ramirez, T. G. Perring, C. J. Carlile, M. Adams, T. J. L. Jones, and B. Hessen, Europhys. Lett. **35**, 127 (1997).
[28] S.-H. Lee, C. Broholm, M. F. Collins, L. Heller, A. P. Ramirez, Ch. Kloc, E. Bucher, R. W. Erwin, and N. Lacevic, Phys. Rev. B **56**, 8091 (1997).
[29] A. Keren, P. Mendels, M. Horvatic, F. Ferrer, Y. J. Uemura, M. Mekata, and T. Asano, Phys. Rev. B **57**, 10 745 (1998).
[30] Y. J. Uemura, A. Keren, K. Kojima, L. P. Le, G. M. Luke, W. D. Wu, Y. Ajiro, T. Asano, Y. Kuriyama, M. Mekata, H. Kikuchi, and K. Kakurai, Phys. Rev. Lett. **73**, 3306 (1994).
[31] V. Elser, Phys. Rev. Lett. **62**, 2405 (1990).
[32] D. S. Greywall, Phys. Rev. B **41**, 1842 (1990).
[33] M. Roger, C. Bauerle, Yu. M. Bunkov, A.-S. Chen, and H. Godfrin, Phys. Rev. Lett. **80**, 1308 (1998).
[34] K. Awaga, T. Okuno, A. Yamaguchi, M. Hasegawa, T. Inabe, Y. Maruyama, and N. Wada, Phys. Rev. B **49**, 3975 (1994).
[35] N. Wada, T. Kobayashi, H. Yano, T. Okuno, A. Yamaguchi, and K. Awaga, J. Phys. Soc. Jpn. **66**, 961 (1997).
[36] J. E. Dutrizac, NATO Conf. Ser. (Hydromet Process. Fund.) **10**, 125 (1984).
[37] M. G. Townsend, G. Longworth, and E. Roudaut, Phys. Rev. B **33**, 4919 (1986).
[38] J. G. Fairchild, Am. Mineral. **18**, 543 (1933).

[39] G. P. Brophy, S. C. Scott, and R. A. Snellgrove, Am. Mineral. **47**, 112 (1962).
[40] J. E. Dutrizac and S. Kaiman, Can. Mineral. **14**, 151 (1975).
[41] J. E. Dutrizac and J. L. Jambor, Hydrometallurgy **17**, 251 (1987).
[42] A. Z. Hrynkiewicz, J. Kubisz, and D. S. Kulgawczuk, J. Inorg. Nucl. Chem. **27**, 2513 (1965).
[43] M. Takano, T. Shinjo, and T. Takada, J. Phys. Soc. Jpn. **30**, 1049 (1971).
[44] M. Takano, T. Shinjo, M. Kiyama, and T. Takada, J. Phys. Soc. Jpn. **25**, 902 (1968).
[45] A. M. Afanasev, V. D. Gorobchenko, D. S. Kulgawczuk, and I. I. Lukashevich, Phys. Status Solidi A **26**, 697 (1974).
[46] D. A. Powers, G. R. Rossman, H. J. Schuger, and H. B. Gray, J. Solid State Chem. **13**, 1 (1975).
[47] A. Keren, K. Kojima, L. P. Le, G. M. Luke, W. D. Wu, Y. J. Uemura, M. Takano, H. Dabkowska, and M. J. P. Gingras, Phys. Rev. B **53**, 6451 (1996).
[48] S. Maegawa, M. Nishiyama, N. Tanaka, A. Oyamada, and M. Takano, J. Phys. Soc. Jpn. **65**, 2776 (1996).
[49] A. S. Wills and A. Harrison, J. Chem. Soc. Faraday Trans. **92**, 2161 (1996).
[50] Wills, A. Harrison, S. A. M. Mentink, T. E. Mason, and Z. Tun, Europhys. Lett. **42**, 325 (1998).
[51] A. S. Wills, Ph.D. thesis, The University of Edinburgh, 1997.
[52] T. Inami, S. Maegawa, and M. Takano, J. Magn. Magn. Mater. **177**, 752 (1998).
[53] S. A. Earle, A. P. Ramirez, and R. J. Cava, Physica B **262**, 199 (1999).
[54] G. S. Oakley, D. Visser, J. Frunzke, K. H. Andersen, A. S. Wills, and A. Harrison, Physica B **267–268**, 142 (1999).
[55] G. S. Oakley, S. Pouget, A. Harrison, J. Frunzke, and D. Visser, Physica B **267–268**, 145 (1999).
[56] J. E. Dutrizac and S. Kaiman, Can. Mineral. **14**, 151 (1976).
[57] J. E. Dutrizac, Metall. Mater. Trans. B **14B**, 531 (1983).
[58] A. Martin and A. Feltz, Z. Anorg. Allg. Chem. **575**, 115 (1989).
[59] C. Härtig, P. Brand, and K. Bohmhammel, Neue Huutte **35**, 205 (1990).
[60] J. T. Szymanski, Can. Mineral. **23**, 659 (1985).
[61] J. Kubisz, Mineral. Pol. **1**, 47 (1970).
[62] A. C. Larson and R. B. Von Dreele, Los Alamos National Laboratory Report No. LAUR 86-748, 1994 (unpublished).
[63] H. A. Levy and S. W. Peterson, J. Chem. Phys. **21**, 365 (1963).
[64] S. B. Hendricks, Am. Mineral. **22**, 773 (1937).
[65] B. E. Warren, Phys. Rev. **59**, 693 (1941).
[66] J. E. Greedan, M. Bieringer, J. Britten, D. M. Giaquinta, and H. C. zur Loye, J. Solid State Chem. **116**, 118 (1995).
[67] A. S. Wills, N. P. Raju, C. Morin, and J. E. Greedan, Chem. Mater. **11**, 1936 (1999).
[68] D. A. Garanin and B. Canals, Phys. Rev. B **59**, 443 (1999).
[69] R. L. Carlin, *Magnetochemistry* (Springer, Berlin, 1986).
[70] A. Harrison, S. J. Clarke, T. E. Mason, and D. Visser, J. Magn. Magn. Mater. **104–107**, 557 (1992).
[71] G. J. Long, G. Longworth, P. Battle, A. K. Cheetham, R. V. Thundathil, and D. Beveridge, Inorg. Chem. **18**, 624 (1970).
[72] J. B. Goodenough, *Magnetism and the Chemical Bond* (Wiley, New York, 1963).
[73] D. L. Huber and W. Y. Ching, Phys. Rev. B **47**, 3220 (1993).